Radiation-Induced Degradation Mechanism of X-Ray SOI Pixel Sensors With Pinned Depleted Diode Structure

Kouichi Hagino, Masatoshi Kitajima, Takayoshi Kohmura, Ikuo Kurachi, *Member, IEEE*, Takeshi G. Tsuru, Masataka Yukumoto, Ayaki Takeda, Koji Mori, Yusuke Nishioka, and Takaaki Tanaka

***Abstract*— The X-ray silicon-on-insulator (SOI) pixel sensor named X-ray pixel (XRPIX) has been developed for the future X-ray astronomical satellite focusing on relativistic universe and cosmic evolution (FORCE). XRPIX is capable of a wide-band X-ray imaging spectroscopy from below 1 keV to a few tens of keV with a good timing resolution of a few tens of μs. However, it had a major issue with its radiation tolerance to the total ionizing dose (TID) effect because of its thick buried oxide layer due to the SOI structure. Although new device structures introducing pinned depleted diodes (PDDs) dramatically improved radiation tolerance, it remained unknown how radiation effects degrade the sensor performance. Thus, this article reports the results of a study of the degradation mechanism of XRPIX due to radiation using device simulations. In particular, mechanisms of increases in dark current and readout noise are investigated by simulation, taking into account the positive charge accumulation in the oxide layer and the increase in the surface recombination velocity at the interface between the sensor layer and the oxide layer. As a result, it is found that the depletion of the buried p-well (BPW) at the interface increases the dark current and that the increase in the sense-node capacitance increases the readout noise.**

***Index Terms*— Astrophysics, radiation effect, silicon-on-insulator (SOI) pixel sensor, X-ray detectors.**

Manuscript received 12 April 2023; revised 9 June 2023 and 14 June 2023; accepted 14 June 2023. Date of publication 16 June 2023; date of current version 18 July 2023. This work was supported in part by the KIOXIA Corporation and by the Japan Society for the Promotion of Science Grant-in-Aid for 22H01269. This work was also supported by the VLSI Design and Education Center (VDEC), the University of Tokyo in collaboration with Cadence Design Systems, Inc., and Mentor Graphics, Inc.

Kouichi Hagino was with the Research Advancement and Management Organization, Kanto Gakuin University, Yokohama 236-8501, Japan. He is now with the Department of Physics, University of Tokyo, Bunkyo, Tokyo 113-0033, Japan, and also with the Research Center for Space System Innovation, Tokyo University of Science, Noda, Chiba 278-8510, Japan (e-mail: kouichi.hagino@phys.s.u-tokyo.ac.jp).

Masatoshi Kitajima is with the Department of Physics, School of Science and Technology, Tokyo University of Science, Noda, Chiba 278-8510, Japan.

Takayoshi Kohmura is with the Research Center for Space System Innovation and the Department of Physics, School of Science and Technology, Tokyo University of Science, Noda, Chiba 278-8510, Japan.

Ikuo Kurachi is with D&S Inc., Hachioji, Tokyo 193-0834, Japan.

Takeshi G. Tsuru is with the Department of Physics, Faculty of Science, Kyoto University, Sakyo, Kyoto 606-8502, Japan.

Masataka Yukumoto, Ayaki Takeda, Koji Mori, and Yusuke Nishioka are with the Department of Applied Physics, Faculty of Engineering, University of Miyazaki, Miyazaki, Miyazaki 889-2155, Japan.

Takaaki Tanaka is with the Department of Physics, Konan University, Kobe, Hyogo 658-8501, Japan.

Color versions of one or more figures in this article are available at https://doi.org/10.1109/TNS.2023.3287130.

Digital Object Identifier 10.1109/TNS.2023.3287130

I. Introduction

WIDE-BAND X-ray observations from a few keV to a few tens of keV are essential for understanding the high-energy universe because of the broadband spectral nature of the nonthermal X-rays emitted from astronomical objects. However, such observations are very difficult because they require X-ray sensors to have low readout noise for low-energy photon detection and high detection efficiency up to high energies. The X-ray silicon-on-insulator (SOI) pixel sensor named X-ray pixel (XRPIX) is a promising X-ray sensor for this purpose [1]. It has been developed for a future wide-band X-ray astronomical satellite focusing on relativistic universe and cosmic evolution (FORCE) aiming for a launch in the early 2030s [2], [3], [4].

XRPIX is a monolithic pixel sensor composed of a high-resistivity silicon sensor and a low-resistivity silicon CMOS circuit bonded with SOI technology. The high resistivity of the sensor layer enables a thick depletion layer of 200–500 μm, resulting in a high detection efficiency of up to a few tens of keV. Although other technologies such as a high-voltage CMOS and a Si strip detector can also have a thick depletion layer, these sensors are not so good in terms of readout noise [5], [6], [7], limiting the detection capability for low-energy X-rays. XRPIX achieved a low readout noise of $10-20e^-$ by introducing the charge-sensitive amplifier (CSA) in the pixel circuit and by reducing the sense-node capacitance with a new device structure of the sensor layer [8], [9]. Such a low-noise performance enabled the detection of low-energy X-rays below 1 keV [10]. In addition, since the pixel circuit of XRPIX is equipped with a self-trigger function [11], it has a good timing resolution of a few tens of μs. This feature enables a background reduction via the anticoincidence technique with active shields, which is essential for astronomical observations in a higher energy band. Thus, XRPIX is an important sensor for achieving wide-band X-ray observations with the FORCE satellite.

One of the major issues in the development of XRPIX is radiation tolerance, especially for the total ionizing dose (TID) effect [12], [13], [14]. This is because of the thick oxide layer called buried oxide (BOX) between the sensor layer and the CMOS circuit layer [15]. When ionizing radiation particles interact with SiO_2 in the BOX, electron–hole pairs are generated, and holes are trapped due to their low mobility

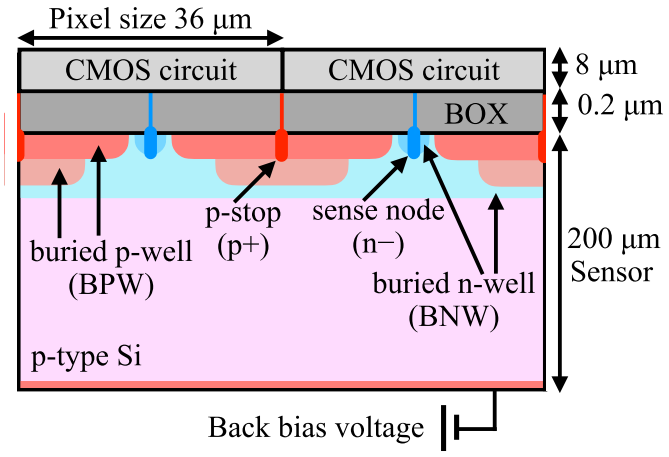

Fig. 1. Schematic picture of one of the latest XRPIXs with PDD structure, XRPIX6E.

in SiO_2. In addition, ionizing radiations increase the interface state density at the Si–SiO_2 boundary. The positive charge accumulation by the trapped holes changes the characteristics of the CMOS circuit and the sensor layer, and the increase in interface state density increases the dark current.

By introducing new device structures, the radiation tolerance of XRPIX has been dramatically improved [13], [16], [17], [18], [19]. However, it remained unknown how residual radiation effects degrade the sensor performance. Thus, in this article, we investigate the radiation-induced degradation mechanism of XRPIX utilizing 3-D device simulations. The rest of the article is organized as follows. In Section II, the specifications of the latest XRPIX are briefly described, and its radiation tolerance based on proton irradiation experiments is summarized. Then, the details of the device simulation are described in Section III, and the degradation mechanisms of the dark current and the spectral performance are discussed in Section IV.

II. Radiation Damage Experiment of XRPIX With PDD Structure

In the previous work [18], we conducted proton irradiation experiments on the latest devices of the XRPIX series named XRPIX6E. We briefly describe the details of the experiments since they are already reported by Hayashida et al. [18].

A. XRPIX With PDD Structure

XRPIX6E has the pinned depleted diode (PDD) structure shown in Fig. 1 [8], [9]. By introducing this structure, XRPIX achieved good spectral performance with an energy resolution of 236 eV at 6.4 keV in full-width at half-maximum (FWHM) [9]. This good performance is primarily because of the pinning of the potential at the Si–SiO_2 interface between the BOX and sensor layer by the p-stop coupled to the buried p-well (BPW). Thanks to the pinning, the BPW reduces the capacitive coupling between the sensor layer and CMOS circuits and suppresses the electrical interference between them. Also, the stepped structure of BPW and buried n-well (BNW) enhances the lateral electric field near the Si–SiO_2 interface, improving the charge collection efficiency.

In addition to the spectral performance, the PDD structure improved the radiation tolerance of XRPIX [18]. By applying the negative bias voltage to the BPW, the negatively pinned potential at the Si–SiO_2 interface compensates for the positive potential of the trapped holes due to the TID effect. The PDD structure also suppresses the effect of increased interface state density due to the TID. It is because the BPW reduces the dark current generation at the Si–SiO_2 interface in the same way as pinned photodiodes in charge-coupled devices and CMOS image sensors [20].

As shown in Fig. 1, the thickness of the sensor layer of XRPIX6E is 200 μm. Its large resistivity of >25 kΩ cm allows full depletion with a back bias voltage of -20 V. XRPIX6E has 48×48 pixels with a pixel size of 36×36 μm. Thus, the imaging area is 1.728×1.728 mm^2, and the total size of XRPIX6E is 4.5×4.5 mm^2 including the peripheral circuits.

B. Measurement of Radiation Damage

In the experiments, two chips of XRPIX6E were irradiated with 6- and 100-MeV proton beams, respectively, at the Heavy Ion Medical Accelerator in Chiba (HIMAC) at the National Institute of Radiological Sciences. The XRPIXs were intermittently irradiated up to total doses of 6 krad(SiO_2) with 6-MeV protons and 40 krad(SiO_2) with 100-MeV, and their performances were evaluated between the irradiations. Hereafter, the total dose is expressed as that for SiO_2 at the BOX layer. During the irradiations, the XRPIXs were cooled down to -65 °C and were operated under the nominal bias voltages: a back bias voltage of -210 V and a bias voltage of -2.0 V for the BPW, which were optimized for the best spectral performance (see [9]).

Although the experimental results demonstrated the improved radiation tolerance of XRPIX, there were still slight performance degradations due to the irradiation [18]. One of the most unexpected results was a dramatic increase in the dark current. Before the irradiation, the dark current was suppressed to very small levels of $\sim$0.1 fA/pixel at -65 °C, which was more than one order of magnitude smaller than that of the previous XRPIX series without the PDD structure. It was naturally expected in the PDD structure. However, after the irradiation with a total dose of 40 krad(SiO_2), the dark current dramatically increased up to 5 fA/pixel at -65 °C. Compared with the previous XRPIX showing only a 10% increase with 5-krad(SiO_2) irradiation [17], this is an unexpectedly rapid increase. The dark current degradation can be affected by the gain degradation described below because it was estimated by measuring the charge flowing into the sense node in the same way as the X-ray charge. Although the effect of gain degradation was a negligibly small value of 1%, it was corrected in the above dark current evaluation.

Spectral performance was also clearly degraded by the proton irradiation with a total dose of more than 10 krad(SiO_2). At 40 krad(SiO_2), the gain decreased by about 1%, corresponding to a 100-eV shift for 10-keV X-rays. The energy resolution at 5.9 keV in FWHM was degraded from 210 eV at 0 rad to

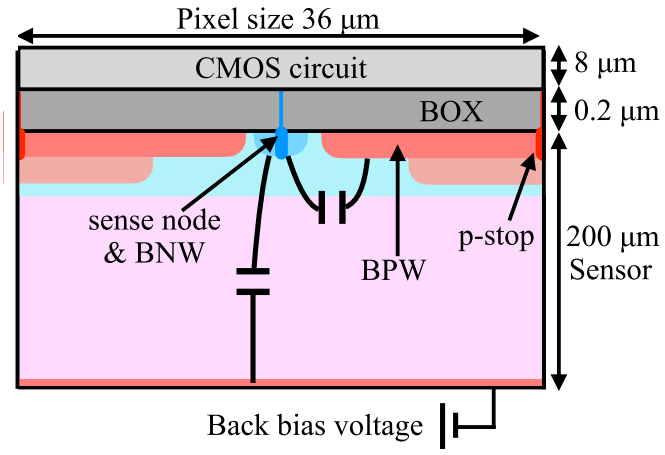

Fig. 2. Schematic picture of the sense-node capacitance of XRPIX with PDD structure.

260 eV at 40 krad(SiO_2). In the previous study, it was found to be primarily due to the degradation of the readout noise [18].

As pointed out by Hagino et al. [17], sense-node capacitance would be one of the keys to understanding these radiation-induced degradations. In particular, a close relationship between the gain degradation and sense-node capacitance was already demonstrated in the case of the previous device of the XRPIX series [17]. Thus, the performance degradation of the latest PDD XRPIX is also expected to be related to the sense-node capacitance.

III. Device Simulations of Radiation Effects in XRPIX With PDD Structure

A. Three-Dimensional Implementation of Device Structure

The sense-node capacitance strongly depends on a 3-D charge distribution in the sensor layer because the capacitance between the sense node and BPW is dominant. As shown in Fig. 2, the distance between the BPW and the BNW around the sense node is less than a few μm, much smaller than the sensor layer thickness of 200 μm. Thus, the sense-node capacitance to the BPW would be more than two orders of magnitude larger than that to the back bias electrode. Since the sense-node capacitance to the BPW is basically in a cylindrical shape, estimation with 2-D simulations is not appropriate, requiring 3-D simulations.

Three-dimensional implementation is also essential for the dark current simulation because the dark current generation via the interface states directly depends on the area of the depleted region at the interface. In particular, since the interface potential pinning with the BPW suppresses such a dark current in the PDD XRPIX, the size of the BPW would be a key to understanding the dark current degradation.

To investigate the mechanism of the radiation-induced degradation of XRPIX6E, we performed 3-D device simulations of the radiation effects in the sensor layer of XRPIX. The simulation was implemented and run using the semiconductor device simulator HyDeLEOS, which is a part of the Technology Computer-Aided Design (TCAD) system HyENEXSS [21], [22]. All the doping structures such as the BPWs, BNWs, p-stop, and sense node were implemented based on the profiles provided by LAPIS Semiconductor Company Ltd. the manufacturer of XRPIX. The bias voltages and temperature were set to be the same as the experimental conditions.

One of the technical difficulties of the 3-D simulation was the number of simulation nodes. The 3-D simulation dramatically increases the number of nodes compared with 2-D simulations due to the addition of a new axis. Thus, the simulation region was limited to a quarter pixel to reduce nodes, resulting in 2×10^5 nodes. In this simulation, the boundary condition is set so that the spatial derivative of the potential is zero at the edge of the simulation region. This condition means that the electric field does not cross the boundary. Thus, cutting at a cross section through the sense node, where no electric field crosses, does not largely affect the simulation result. In fact, the simulated sense-node capacitance with a quarter pixel is consistent with that with an entire pixel with an accuracy of less than 0.1%.

B. Modeling of Radiation Effects

We implemented two radiation effects of TID: positive charge accumulation in the BOX and an increase in interface state density at the Si–SiO_2 interface between the sensor layer and the BOX. Here, it should be noted that the effect of the interface state at the backside is negligible because a highly doped p+ layer is formed at the back side [10], suppressing the dark current generation from the backside interface. The implementation was done in almost the same manner as Kitajima et al. [19]. The charge accumulation was simply modeled by placing fixed charges Q_{BOX} at the nodes adjacent to the Si–SiO_2 interface in the BOX. The BOX charge was increased as a function of total dose D [15]. The increase in interface state density was modeled as an increase in the surface recombination velocity $S \equiv \upsilon \mathrm{th} \sigma N_{\mathrm{it}}$, where υth is the thermal velocity of carriers, σ is the capture cross section of carriers, and N_{it} is the interface state density [23]. This modeling, in which the increase in the interface state density is treated by the single parameter S, is sufficient for describing the contribution to the dark current increase on which this work focuses.

In modeling the radiation effects, there were three undetermined parameters: the amount of BOX charge $Q_{\mathrm{BOX}}(D)$, surface recombination velocity $S(D)$, and Shockley–Read–Hall (SRH) recombination lifetime τ [24]. Here, $S(D)$ and $Q_{\mathrm{BOX}}(D)$ are functions of total dose D. Since the fixed charge is also generated during the wafer process, the BOX charge before the irradiation was assumed to be $Q_{\mathrm{BOX}}(0) = 2.0 \times 10^{11}$ cm^{-2}, following the previous works [17], [19], [25], [26]. Also, the value of surface recombination velocity before the irradiation was assumed to be a typical value of $S(0) = 100$ cm/s (e.g., [27]). The values of SRH recombination lifetime were chosen to reproduce the experimental value of dark current before the irradiation. It is justified by the fact that the dark current before the irradiation is dominated by that generated via the SRH recombination because the potential pinning by the BPW suppresses the dark current via interface

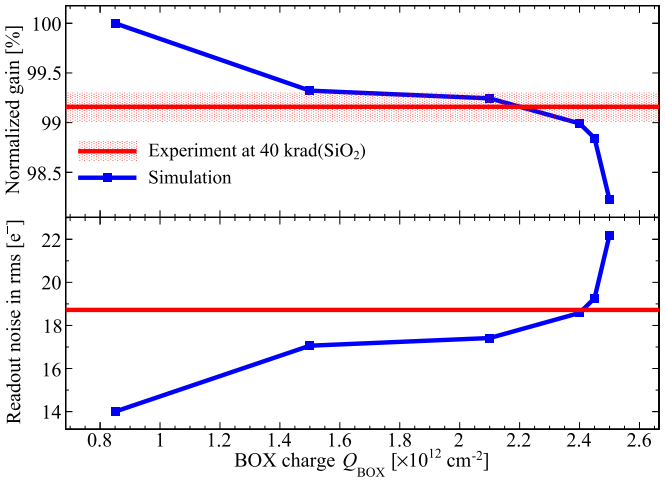

Fig. 3. Dependence on the BOX charge Q_{BOX} of the gain (top panel) and readout noise (bottom panel) based on the device simulation. The red-shaded region indicates the uncertainty of the experimental data.

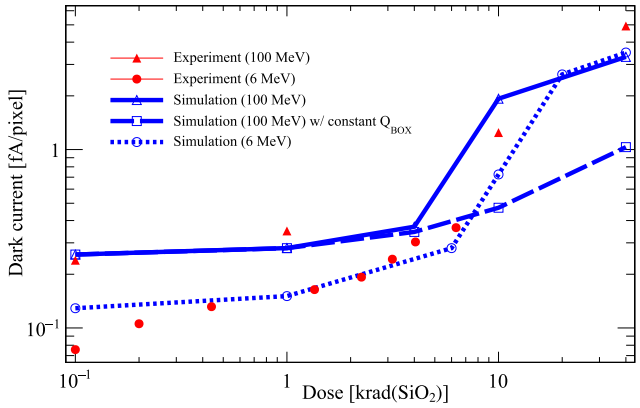

Fig. 4. Simulated dark current as a function of the total dose (blue solid line and blue dotted line), compared with experimental data (red triangle and filled circle). The experimental data are the same as those presented in Hayashida et al. [18]. For discriminating the effects of the increases in BOX charge Q_{BOX} and surface recombination velocity S, the simulated dark current with a constant BOX charge $Q_{\mathrm{BOX}} = 2.0 \times 10^{11}$ cm^{-2} was also shown in a blue dashed line.

states. The chosen values of the SRH recombination lifetime were $\tau_n \simeq 400$ μs for electrons and $\tau_p \simeq 10$ μs for holes for the 100-MeV proton experiment. For the 6-MeV experiment, $\tau_n \simeq 800$ μs and $\tau_p \simeq 20$ μs were chosen. It should be noted that these values do not necessarily require the difference in SRH lifetime between these devices, but also include the effect of experimental environments such as the light leak or electric noise.

The dose dependences of $Q_{\mathrm{BOX}}(D)$ and $S(D)$ were assumed to be simple linear functions [15], [28]. Since the values at 0 rad were already determined, we then chose values at 40 krad(SiO_2) for the 100-MeV proton experiment and linearly interpolated these values. In the parameter choice, it should be noted that the dark current depends on both Q_{BOX} and S, while the sense-node capacitance depends only on Q_{BOX}. Thus, the BOX charge at 40 krad(SiO_2) was first determined to be $Q_{\mathrm{BOX}} = 2.4 \times 10^{12}$ cm^{-2}. As shown in Fig. 3, this value was chosen to reproduce the experimental results of gain and readout noise, which depend on the sense-node capacitance. Then, by comparing with the experimental results of dark current, the surface recombination velocity at 40 krad(SiO_2) was determined to be $S = 5.0 \times 10^5$ cm/s.

The chosen values of Q_{BOX} and S at 40 krad(SiO_2) are reasonable compared with the previous works and literature. According to Schwank et al. [15], the BOX charge is written as

$$Q_{\mathrm{BOX}} = 8.1 \times 10^{12} \times f \times \left(\frac{D}{\mathrm{rad}}\right) \times \left(\frac{t_{\mathrm{BOX}}}{\mathrm{cm}}\right) \mathrm{cm}^{-2} = 6.5 \times 10^{12} \times f \ \mathrm{cm}^{-2} \quad (1)$$

where $D = 40$ krad(SiO_2) is the total dose, $t_{\mathrm{BOX}} = 0.2$ μm is the thickness of the BOX, and f is the fraction of unrecombined holes (charge yield). The charge yield f depends on the electric field strength in the BOX and the linear energy transfer (LET) of the ionizing particle. According to Oldham and McGarrity [29] and Paillet et al. [30], a charge yield of $f = 0.2 - 0.4$ is reasonable for 100-MeV protons with an LET of 6.0 MeV cm^2/g and an electric field strength of ~ 0.1 MV/cm. Thus, the determined value of the BOX charge of $Q_{\mathrm{BOX}} = 2.4 \times 10^{12}$ cm^{-2} is acceptable. On the other hand, the surface recombination velocity $S = 5.0 \times 10^5$ cm/s at 40 krad(SiO_2) determined in this work roughly matches that of $S = 1.7 \times 10^5$ cm/s at 10 krad(SiO_2) determined in the previous work [19].

In addition to the simulations for the 100-MeV proton experiment described above, simulations with a slightly smaller BOX charge Q_{BOX} were also performed to mimic the 6-MeV proton experiment. Although the literature does not provide actual measurements of the charge yield for 6-MeV protons [29], [30], it should be smaller than that for 100-MeV protons because of its larger LET. Thus, a charge yield of $f = 0.2$ was assumed for the 6-MeV proton experiment.

IV. Degradation Mechanism Based on the Device Simulation

A. Simulated Dark Current and Its Degradation Mechanism

Fig. 4 shows the simulated dark current as a function of the total dose. Compared with the experimental data reported by Hayashida et al. [18], the simulated dark current reproduces the experiments within a factor of two. Although it does not accurately reproduce the data, the factor of two is relatively good compared with the increase of as much as one order of magnitude in the experimental data. Thus, this simulation can be considered to have enough capability to qualitatively investigate the physics behind the large increase in the dark current.

To discriminate the effects of the BOX charge and interface states, the blue dashed line in Fig. 4 shows the simulated dark current in a case if the BOX charge remains unchanged at the preirradiation value of $Q_{\mathrm{BOX}} = 2.0 \times 10^{11}$ cm^{-2}. In this additional simulation, the increase in surface recombination velocity S due to the increase in interface state density was set to the same values as in the original simulation. Thus, a discrepancy between this additional simulation and the original one demonstrates the effects of BOX charge,

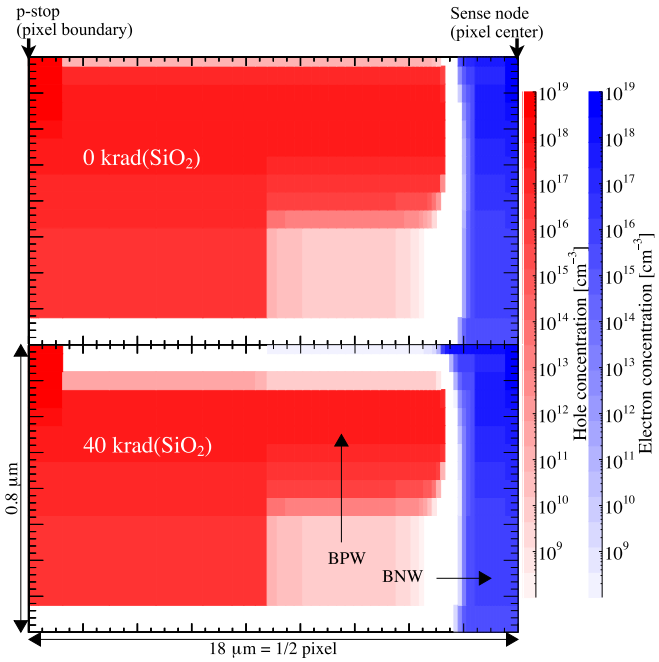

Fig. 5. Two-dimensional maps of the hole (red) and electron (blue) concentrations at 0 rad (top panel) and 40 krad(SiO_2) (bottom panel). These maps show a very vicinity 0.8-μm range from the BOX–sensor interface located at the top edge of each panel. The top edge of each panel corresponds to the interface.

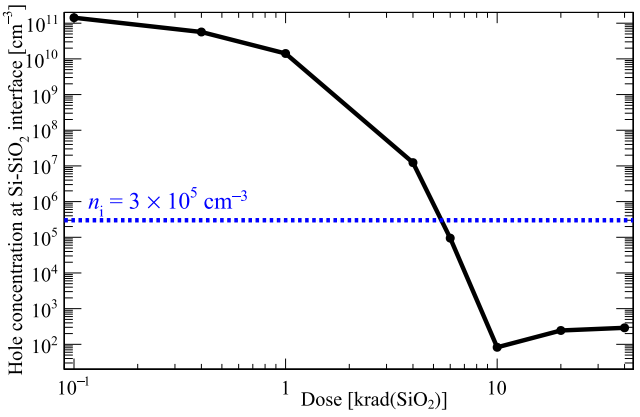

Fig. 6. Hole concentrations at the Si–SiO_2 interface between the sensor and the BOX as a function of the total dose. The intrinsic carrier density at the interface is also plotted by the blue horizontal dotted line.

clearly indicating the importance of the BOX charge in the degradation mechanism of dark current.

The BOX charge should affect the carrier distribution near the interface between the sensor and the BOX. Fig. 5 shows 2-D maps of hole and electron concentrations near the interface at 0 and 40 krad(SiO_2). The figure clearly shows that the BOX charge due to the radiation depletes the interface, which should have been filled with holes to suppress the dark current. The positive potential of the BOX charge pushed holes away from the interface, depleting the interface.

Dose dependence of the hole concentrations at the interface shown in Fig. 6 provides a better understanding of the behavior of the simulated dark current. According to Teranishi et al. [20], dark current due to the interface states

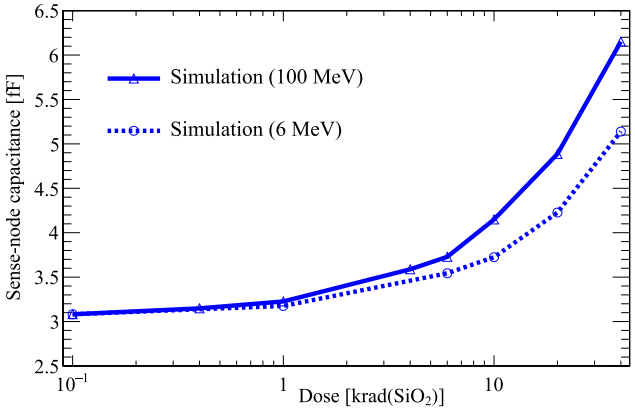

Fig. 7. Simulated sense-node capacitance as a function of the total dose.

is suppressed to $U \leq Sn_i^2/p$ for $p \gg n_i$, while it becomes as large as $U \simeq Sn_i/2$ for $p \ll n_i$. Here, U is the generation rate of carriers in a unit volume, p is the hole concentration, and n_i is the intrinsic carrier density. In this simulation, the value of the intrinsic carrier density at the interface at -65 °C is $n_i \simeq 3 \times 10^5$ cm^{-3}. Thus, because the hole concentration rapidly changes from $p \gg n_i$ to $p \ll n_i$ around 6 krad(SiO_2), the simulated dark current also dramatically increases at 4–10 krad(SiO_2) as shown in Fig. 4. After the dramatic increase, the increase in dark current slows down because the interface is fully depleted above 10 krad(SiO_2) and the hole concentration becomes unchanged.

The depletion of the BPW at the interface was unexpected but not surprising. The positive potential ΔV required to form a depletion layer with a thickness of $W \sim 0.5$ μm is calculated as $\Delta V = eN_A W^2/2\varepsilon_{\mathrm{Si}} \simeq 2$ V, using the acceptor concentration near the interface of $N_A \simeq 10^{16}$ cm^{-3} and the permittivity of Si of $\varepsilon_{\mathrm{Si}} \simeq 1.0 \times 10^{-12}$ F cm^{-1}. The BOX charge due to the irradiation can easily create such a positive potential of a few volts. Actually, in this simulation, the potential at the interface increased by 3.1 V with a total dose of 40 krad(SiO_2).

In summary, the dark current increases with the following mechanism. First, the BOX charge and interface state density increase due to the irradiation. Then, the interface states gradually increase the dark current. In addition, the depletion of the BPW by the BOX charge disables the dark current suppression of the BPW, resulting in a dramatic increase in the dark current. Thus, to achieve more radiation tolerance, it is important to improve the device structure to avoid the depletion of the BPW.

B. Sense-Node Capacitance and Its Effects on Gain and Noise Performance

Fig. 7 shows the sense-node capacitance obtained by the device simulation. The simulated value of $C_D = 3.1$ fF at 0 rad was consistent with experimental results of capacitance measurement of test chips having the same structure as XRPIX6E. This capacitance measurement was performed by directly probing the sense node of the test chip, where the sense nodes of each pixel are connected to each other

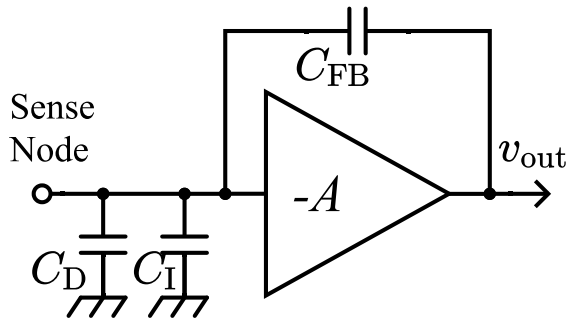

Fig. 8. Schematic of the equivalent circuit of the CSA in the pixel circuit. The sense-node capacitance C_D affects the magnitudes of noise and output signal (i.e., gain).

and also to the pad. In the figure, by increasing the BOX charge, the simulated sense-node capacitance increased monotonically up to $C_D = 6.2$ fF at 40 krad(SiO_2). The mechanism of the capacitance increase is understandable from Fig. 5. Since the positive potential of the BOX charge attracts electrons, the BNW around the sense node enlarges with the irradiation, narrowing the depleted region between the BPW and the BNW. Thus, the sense-node capacitance increases with the BOX charge due to the irradiation.

The increase in sense-node capacitance affects the spectral performance, such as noise and gain, through the CSA, the first amplifier in the pixel circuit of XRPIX. Fig. 8 shows a schematic of the equivalent circuit of the CSA in XRPIX, where $C_{\mathrm{FB}} = 2.7$ fF and $C_I = 4.0$ fF are the feedback capacitance and the input capacitance of the CSA, respectively. The design value of the open-loop gain is approximately $A \simeq 108$ [31]. In this equivalent circuit, the gain of the CSA defined as output voltage relative to input charge from the sense node is written as

$$G = \frac{A}{C_D + C_I + (A+1)C_{\mathrm{FB}}}. \tag{2}$$

In the ideal case with an infinite open-loop gain of $A = \infty$, the gain depends only on the feedback capacitance as $G \simeq 1/C_{\mathrm{FB}}$. However, with the actual value of $A \simeq 108$, the effect of the sense-node capacitance C_D is not negligible.

The gain affected by the increasing sense-node capacitance is shown in Fig. 9. As the sense-node capacitance increases with irradiation (see Fig. 7), the gain also monotonically decreases. Compared with the experimental data, the gain calculated with the simulated sense-node capacitance well reproduces the experiments, indicating the gain degradation due to the irradiation is primarily caused by the increase in the sense-node capacitance. This is the same mechanism as in the case of the previous XRPIX [17].

The sense-node capacitance also affects the noise performance of XRPIX through the CSA. According to Kamehama et al. [8], under the assumption that the flicker noise is dominant rather than the thermal noise, the input-referred noise N of the CSA approximately depends on the sense-node capacitance C_D as

$$N \propto \frac{1}{G}\frac{C_D + C_I + C_{\mathrm{FB}}}{C_{\mathrm{FB}}}. \tag{3}$$

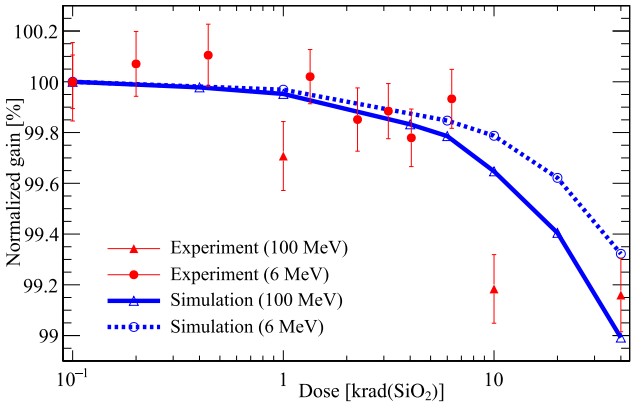

Fig. 9. Gain calculated from the simulated sense-node capacitance as a function of the total dose (blue solid line and blue dotted line), compared with experimental data (red triangle and filled circle). The experimental data are the same as those presented in Hayashida et al. [18]. The vertical axis is normalized with the preirradiation value.

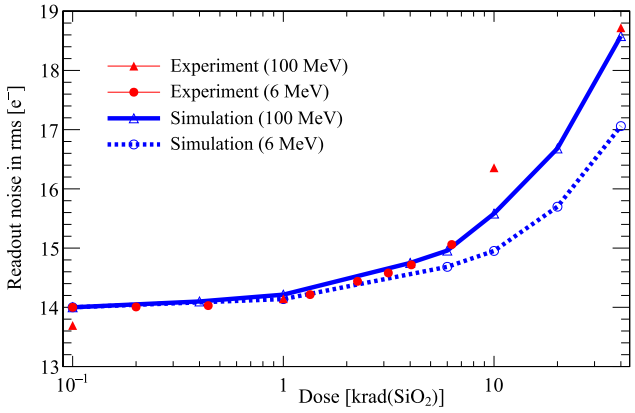

Fig. 10. Readout noise calculated from the simulated sense-node capacitance as a function of the total dose (blue solid line and blue dotted line), compared with experimental data (red triangle and filled circle). In the experimental data shown here, the shot noise of the dark current is subtracted from the original plot presented in Hayashida et al. [18].

It should be noted that this formula omits logarithmic dependence on $(C_D + C_I + C_{\mathrm{FB}})/C_{\mathrm{FB}}$ because its contribution is negligible. Since the proportional coefficient of this formula includes unknown parameters such as the flicker noise coefficient of the transistor, this work focused only on the proportional relation depending on the sense-node capacitance under the above assumptions.

Fig. 10 shows the increase in the readout noise calculated with (3) based on the simulated sense-node capacitance. Here, the proportional coefficient of (3) was chosen to match the experimental value at preirradiation. Similar to the gain degradation, the readout noise calculated with the simulated sense-node capacitance successfully reproduces the noise degradation in the experiment. Thus, this result indicates the increase in the sense-node capacitance is also dominant in the radiation-induced degradation of the readout noise of XRPIX.

The above discussions exhibit the importance of the increase in the sense-node capacitance for spectral performance, particularly for degradations of gain and readout noise. Thus, for radiation tolerance, it is important to keep the sense-node

capacitance as low as possible after the irradiation. We are now investigating new device structures for more improvement in the performance of XRPIX. The results of such studies will be presented in future work.

V. Conclusion

This article investigated the radiation-induced degradation mechanism of the X-ray SOI pixel sensor "XRPIX" using 3-D device simulations. The simulations roughly matched the measured dark current degradation, and the gain and readout noise calculated from the simulated sense-node capacitance successfully reproduced those obtained in the experiments. These device simulations also revealed the radiation-induced degradation mechanism of XRPIX, especially for the dark current, gain, and readout noise. The dramatic increase in the dark current of XRPIX induced by the irradiation was primarily due to the depletion of the BPW formed at the $Si–SiO_2$ interface. In the degradation of gain and readout noise, the sense-node capacitance played an important role. The sense-node capacitance increased due to the enlargement of the BNW around the sense node; it reduced the gain and increased the readout noise through the CSA in the pixel circuit.

Acknowledgment

The authors would like to acknowledge the valuable advice and great work of the personnel of LAPIS Semiconductor Company Ltd.

References

[1] T. G. Tsuru et al., "Kyoto's event-driven X-ray astronomy SOI pixel sensor for the FORCE mission," *Proc. SPIE*, vol. 10709, Aug. 2018, Art. no. 107090H.

[2] K. Mori et al., "A broadband X-ray imaging spectroscopy in the 2030s: The FORCE mission," *Proc. SPIE*, vol. 12181, Aug. 2022, Art. no. 1218122.

[3] K. Nakazawa et al., "The FORCE mission: science aim and instrument parameter for broadband X-ray imaging spectroscopy with good angular resolution," *Proc. SPIE*, vol. 10699, Jul. 2018, Art. no. 106992D.

[4] K. Mori et al., "A broadband X-ray imaging spectroscopy with high-angular resolution: The FORCE mission," *Proc. SPIE*, vol. 9905, Aug. 2016, Art. no. 99051O.

[5] I. Peric et al., "High-voltage CMOS active pixel sensor," *IEEE J. Solid-State Circuits*, vol. 56, no. 8, pp. 2488–2502, Aug. 2021.

[6] I. Brewer et al., "Developing the future of gamma-ray astrophysics with monolithic silicon pixels," *Nucl. Instrum. Methods Phys. Res. A, Accel. Spectrom. Detect. Assoc. Equip.*, vol. 1019, Dec. 2021, Art. no. 165795.

[7] S. Ishikawa et al., "Fine-pitch semiconductor detector for the FOXSI mission," *IEEE Trans. Nucl. Sci.*, vol. 58, no. 4, pp. 2039–2046, Aug. 2011.

[8] H. Kamehama et al., "A low-noise X-ray astronomical silicon-on-insulator pixel detector using a pinned depleted diode structure," *Sensors*, vol. 18, no. 2, p. 27, Dec. 2017.

[9] S. Harada et al., "Performance of the silicon-on-insulator pixel sensor for X-ray astronomy, XRPIX6E, equipped with pinned depleted diode structure," *Nucl. Instrum. Methods Phys. Res. A, Accel. Spectrom. Detect. Assoc. Equip.*, vol. 924, pp. 468–472, Apr. 2019.

[10] R. Kodama et al., "Low-energy X-ray performance of SOI pixel sensors for astronomy, 'XRPIX,"' *Nucl. Instrum. Methods Phys. Res. A, Accel. Spectrom. Detect. Assoc. Equip.*, vol. 986, Jan. 2021, Art. no. 164745.

[11] A. Takeda et al., "Design and evaluation of an SOI pixel sensor for trigger-driven X-ray readout," *IEEE Trans. Nucl. Sci.*, vol. 60, no. 2, pp. 586–591, Apr. 2013.

[12] K. Hara et al., "Radiation hardness of silicon-on-insulator pixel devices," *Nucl. Instrum. Methods Phys. Res. A, Accel. Spectrom. Detect. Assoc. Equip.*, vol. 924, pp. 426–430, Apr. 2019.

[13] K. Yarita et al., "Proton radiation damage experiment for X-ray SOI pixel detectors," *Nucl. Instrum. Methods Phys. Res. A, Accel. Spectrom. Detect. Assoc. Equip.*, vol. 924, pp. 457–461, Apr. 2019.

[14] K. Hagino et al., "Single event tolerance of X-ray silicon-on-insulator pixel sensors," *J. Astronomical Telescopes, Instrum., Syst.*, vol. 8, no. 4, Oct. 2022, Art. no. 046001.

[15] J. R. Schwank et al., "Radiation effects in MOS oxides," *IEEE Trans. Nucl. Sci.*, vol. 55, no. 4, pp. 1833–1853, Aug. 2008.

[16] K. Mori et al., "Total ionizing dose effects on the SOI pixel sensor for X-ray astronomical use," *Nucl. Instrum. Methods Phys. Res. A, Accel. Spectrom. Detect. Assoc. Equip.*, vol. 924, pp. 473–479, Apr. 2019.

[17] K. Hagino et al., "Radiation damage effects on double-SOI pixel sensors for X-ray astronomy," *Nucl. Instrum. Methods Phys. Res. A, Accel. Spectrom. Detect. Assoc. Equip.*, vol. 978, Oct. 2020, Art. no. 164435.

[18] M. Hayashida et al., "Proton radiation hardness of X-ray SOI pixel sensors with pinned depleted diode structure," *J. Astronomical Telescopes, Instrum., Syst.*, vol. 7, no. 3, Aug. 2021, Art. no. 036001.

[19] M. Kitajima et al., "X-ray radiation damage effects on double-SOI pixel detectors for the future astronomical satellite FORCE," *J. Astronomical Telescopes, Instrum., Syst.*, vol. 8, no. 2, Jun. 2022, Art. no. 026007.

[20] N. Teranishi, "Effect and limitation of pinned photodiode," *IEEE Trans. Electron Devices*, vol. 63, no. 1, pp. 10–15, Jan. 2016.

[21] *3D TCAD Simulator HyENEXSS ver. 8.5K*, Keio Univ. TCAD Research and Development Center, Tokyo, Japan, 2019.

[22] N. Kotani, "TCAD in Selete," in *Proc. Int. Conf. Simulation Semiconductor Processes Devices, (SISPAD)*, Leuven, Belgium, 1998, pp. 3–7.

[23] S. Sze, *Physics of Semiconductor Devices*. Hoboken, NJ, USA: Wiley, 2002.

[24] W. Shockley and W. T. Read, "Statistics of the recombinations of holes and electrons," *Phys. Rev.*, vol. 87, no. 5, pp. 835–842, Sep. 1952.

[25] H. Matsumura et al., "Improving charge-collection efficiency of SOI pixel sensors for X-ray astronomy," *Nucl. Instrum. Methods Phys. Res. A, Accel. Spectrom. Detect. Assoc. Equip.*, vol. 794, pp. 255–259, Sep. 2015.

[26] K. Hagino et al., "Sub-pixel response of double-SOI pixel sensors for X-ray astronomy," *J. Instrum.*, vol. 14, no. 10, Oct. 2019, Art. no. C10023.

[27] B. Imangholi, F. L. Lie, H. G. Parks, and A. J. Muscat, "Effect of deep-level defects on surface recombination velocity at the interface between silicon and dielectric films," *IEEE Trans. Electron Devices*, vol. 57, no. 4, pp. 877–889, Apr. 2010.

[28] N. S. Saks, M. G. Ancona, and J. A. Modolo, "Generation of interface states by ionizing radiation in very thin MOS oxides," *IEEE Trans. Nucl. Sci.*, vol. NS-33, no. 6, pp. 1185–1190, Dec. 1986.

[29] T. R. Oldham and J. M. McGarrity, "Comparison of ^{60}Co response and 10 KeV X-ray response in MOS capacitors," *IEEE Trans. Nucl. Sci.*, vol. NS-30, no. 6, pp. 4377–4381, Dec. 1983.

[30] P. Paillet et al., "Comparison of charge yield in MOS devices for different radiation sources," *IEEE Trans. Nucl. Sci.*, vol. 49, no. 6, pp. 2656–2661, Dec. 2002.

[31] A. Takeda et al., "Spectroscopic performance improvement of SOI pixel detector for X-ray astronomy by introducing double-SOI structure," *J. Instrum.*, vol. 15, no. 11, Nov. 2020, Art. no. P11001.